Heliyon 11 (2025) e41960

Contents lists available at ScienceDirect

Heliyon

journal homepage: www.cell.com/heliyon

Research article

Small extracellular vesicles derived from miRNA-486 overexpressed dental pulp stem cells mitigate high altitude pulmonary edema through PTEN/PI3K/AKT/eNOS pathway

Changyao Wang [a,1], Zhuang Mao [a,1], Drolma Gomchok [b,c,1], Xue Li [a], Huifang Liu [b,c], Jingyuan Shao [a], Hu Cao [a], Guanzhen Xue [b,c], Lin Lv [a], Junzhao Duan [a], Tana Wuren [b,c,**], Hua Wang [a,*]

[a] Beijing Institute of Radiation Medicine, Beijing, 100850, China
[b] Research Center for High Altitude Medicine, Qinghai University, Xi'ning, 810008, China
[c] Key Laboratory for Application of High-Altitude Medicine, Qinghai University, Xi'ning, 810008, China

ARTICLE INFO

Keywords:
High-altitude pulmonary edema
Extracellular vesicles
miR-486
Oxidative stress

ABSTRACT

High altitude pulmonary edema (HAPE) is a life-threatening, non-cardiogenic pulmonary edema characterized by rapid onset and high mortality. Extracellular vesicles of mesenchymal stem cells are used in the treatment of a variety of lung diseases, but their use in HAPE remains underreported. This study explores the therapeutic potential of miRNA-486 modified extracellular vesicles from dental pulp stem cells ($sEV^{miR-486}$) against HAPE, aiming to decipher the associated molecular mechanisms. The rat HAPE model was established by exposing subjects to a simulated high-altitude, low-oxygen environment within a specialized chamber. The HAPE-afflicted rats received sEV^{Null} and $sEV^{miR-486}$ intravenously, and the therapeutic effect was assessed through histopathological analysis, pulmonary artery pressure, lung water content, as well as markers of oxidative stress and inflammation. To supplement in vivo findings, pulmonary microvascular endothelial cells (PMVEC) were stressed with cobalt chloride to emulate hypoxic damage, and then treated with sEV^{Null} and $sEV^{miR-486}$ to unravel the mechanism of action. The sEV^{Null} mitigated pathological changes in the lungs, reduced pulmonary artery pressure and lung water content, and alleviated oxidative stress and inflammatory responses in cases of HAPE. Moreover, sEV^{Null} enhanced vascular reactivity and restored pulmonary permeability and tight junction integrity, these effects were intensified by miRNA-486 overexpression. Notably, $sEV^{miR-486}$ attenuated oxidative damage in hypoxic PMVEC cells by modulating the PTEN/PI3K/Akt/eNOS signaling pathway. miRNA-486 fortified DPSC-sEVs intervention as a novel and potent treatment strategy for HAPE.

* Corresponding author.
** Corresponding author. Research Center for High Altitude Medicine, Qinghai University, Xi'ning, 810008, China.
E-mail addresses: tana.wuren@qhu.edu.cn (T. Wuren), 18511712135@163.com (H. Wang).
[1] These authors contributed equally to this study.

https://doi.org/10.1016/j.heliyon.2025.e41960
Received 29 July 2024; Received in revised form 1 January 2025; Accepted 13 January 2025
Available online 14 January 2025

1. Introduction

High altitude pulmonary edema (HAPE) is a non-cardiogenic form of edema that affects unacclimatized individuals at elevations above 2500 m [1]. Typically manifesting 2–3 days after sudden altitude exposure, HAPE is characterized by increased pulmonary artery pressure, hypoxic pulmonary vasoconstriction, enhanced alveolar capillary permeability, and hypoxemia [2]. Although treatments such as vasodilators, corticosteroids, hormones, supplemental oxygen, and rapid descent can effectively mitigate HAPE [3], the condition maintains a mortality rate of up to 40 % when diagnosis and treatment are delayed [4]. The necessity for reliable predictors and treatment modalities remains critical, as current options are insufficient.

Several studies have demonstrated that rats exposed to acute low-pressure hypoxia exhibit increased levels of reactive oxygen species (ROS), leading to oxidative stress and consequential enhancements in transvascular leakage [5]. Pulmonary microvascular endothelial cells (PMVEC), characterized by heightened permeability, are implicated as a central cellular mechanism contributing to vascular leakage and the pathogenesis of HAPE [6]. Recent findings suggest that mesenchymal stem cells (MSCs) may mitigate inflammation, apoptosis, and oxidative stress while fostering angiogenesis, thereby promoting alveolar fluid clearance, minimizing damage to lung endothelial and epithelial cells, and ultimately attenuating lung injury [7–10]. Dental pulp stem cells (DPSCs) are a type of mesenchymal stem cells derived from the cranial neural crest and extracted from the discarded teeth, which characterized by a wide range of sources and high proliferation rate. Meanwhile, some studies indicated that DPSCs had the ability to inhibit inflammation, anti-aging, promote angiogenesis, and inhibit tumor proliferation, invasion and metastasis [11–14]. The contribution of paracrine factors and extracellular vesicles are instrumental in mediating these protective effects.

Extracellular vesicles (EVs) are lipid bilayer-encased particles that transport biologically active molecules, including proteins, RNAs, and microRNAs [15]. These vesicles have the capability to deliver their cargo to target cells, thereby modulating cellular functions and facilitating tissue repair mechanisms [16,17]. EVs are classified into two principal categories: exosomes and microvesicles, with small EVs (sEVs) under 200 nm predominantly constituting exosomes, and larger EVs, exceeding 200 nm, mainly comprising microvesicles [18]. Compared to MSCs, MSC-derived sEVs (MSC-sEVs) offer benefits such as reduced immunogenicity, ease of preparation, high stability, and uncomplicated storage [19]. Multiple studies have demonstrated that MSC-sEVs can mitigate lung injury through the reduction of inflammation [20], the attenuation of pulmonary artery pressure [21], and the enhancement of cell migration and angiogenesis [22].

MicroRNAs (miRNAs) are short, non-coding RNA sequences, typically 22–25 nucleotides in length. They are involved in the post-transcriptional regulation of almost all cellular processes and play consequently important roles in the development of many diseases. Accordingly, miRNAs have attracted great interest as potential novel tools for diagnosis and even therapy [23]. Engineered sEVs that modify either the composition or expression levels of miRNAs in their cargo can enhance therapeutic efficacy. For instance, sEVs derived from human umbilical cord mesenchymal stem cells that overexpress miR-199a-5p have been demonstrated to mitigate oxidative stress in sulfur mustard (SM) induced acute lung injury. This therapeutic effect is achieved by downregulating Caveolin1 and activating key antioxidative pathways involving nuclear factor E2-related factor 2 (Nrf2), heme oxygenase-1 (HO-1), and NAD(P)H Dehydrogenase Quinone 1 (NQO1) [24]. Furthermore, miR-486-5p is implicated in regulating cell proliferation, migration, angiogenesis, apoptosis, and other processes [25]. Studies have identified that miRNA-486-5p can protect against endothelial dysfunction by curbing inflammation and oxidative stress [26]. In a previous study in our lab, miR-486 was found to mediate hypoxia-induced vasoreactivity and promote the proliferation and survival of BM-MSCs by regulating the PTEN/PI3K/AKT signaling pathway [27].

In this study, we sought to investigate the potential therapeutic effect of miRNA-486-overexpressed sEVs derived from DPSCs ($sEV^{miR-486}$) on an experimental rat HAPE model, which simulated acute hypobaric hypoxia and established by exposing rats to a hypobaric chamber. In addition, $CoCl_2$ induced hypoxic damage model of PMVEC was used to elucidate the possible mechanisms.

2. Materials and methods

2.1. Cell culture

PMVEC were obtained from BLUEFBIO (Shanghai, China). These cells were maintained in Dulbecco's Modified Eagle's Medium (DMEM; Gibco, Thermo Fisher Scientific, Waltham, MA, USA), supplemented with 10 % fetal bovine serum (FBS; Gibco). To induce a hypoxic injury model, PMVECs were exposed to 200 μM cobalt chloride (Sigma, CA, USA).

DPSCs were generously provided by Beijing SH Biotechnology. These DPSCs were maintained in AM-V serum-free medium specifically formulated for mesenchymal stem cells, supplied by TBD in Tianjin, China. The cells were infected with 70 MOI Ad.miR486, a replication-incompetent adenoviral vector designed to express miRNA-486, or with Ad.Null, which is also a replication-incompetent adenoviral vector but does not express any exogenous genes. Subsequently, the culture medium was harvested to collect small extracellular vesicles overexpressing miRNA-486 ($sEV^{miR-486}$) as well as the control small extracellular vesicles (sEV^{Null}).

2.2. Isolation and characterization of sEVs

In this study, sEVs were isolated using a differential ultracentrifugation protocol. Initially, culture medium from 4-day cultures of DPSCs infected with Ad.Null and DPSCs overexpressing miRNA-486 was harvested. This medium was subjected to sequential centrifugation: first at 300g for 10 min to remove dead cells, then at 2000g for 20 min to eliminate apoptotic bodies, followed by 10,000g for 30 min to clear cell debris. Subsequently, sEVs were purified through an ultracentrifuge (XPN-80, Beckman Coulter, USA) at 100,000g for 70 min, repeated twice. The resulting sEVs pellets were resuspended in phosphate-buffered saline (PBS). All procedures

were conducted at 4 °C to ensure integrity, and the isolated sEVs were either stored at −80 °C or utilized immediately for further experiments.

Nanoparticle Tracking Analysis (NTA) facilitated by the ZetaView PMX 110 (Particle Metrix) was employed to ascertain the concentration and size distribution of sEVs. Specimens were suitably diluted before being introduced into the sample chamber. Subsequent data acquisition was analyzed with the integrated ZetaView software (version 8.04.02 SP2).

The ultrastructure of sEVs was visualized using transmission electron microscopy. Images of sEVs were acquired using a Hitachi HT7800 electron microscope (RuliTEM, HT7800).

PKH26 (MedChemExpress, HY-D1451) dye was used to bind to sEVs. PKH26-labeled sEVs was added into PMVEC cells or injected into BALB/c mice via tail vein. Images of cells and animals ingesting sEVs were acquired by laser confocal microscopy and in vivo imaging system.

2.3. In vitro cellular experiment grouping and protocols

To study the function of $sEV^{miR-486}$, PMVEC cells were divided into four groups: a. Control group: PMVEC cells were not subjected to any additional treatments; b. Hypoxia group: PMVEC cells were exposed to 200 μM $CoCl_2$ for 24 h to induce hypoxic injury; c. sEV^{null} group: PMVEC cells were treated with 200 μM $CoCl_2$ for 12 h, and then 20 μg of sEV^{null} was added; d. $sEV^{miR-486}$ group: PMVEC cells were treated with 200 μM $CoCl_2$ for 12 h, and then 20 μg of $sEV^{miR-486}$ was added.

To further elucidate the function of miRNA-486, PMVEC cells were divided into four groups: a. Mimic-NC group: PMVEC cells were treated with 200 μM $CoCl_2$ for 12 h, followed by transfection of 15 nM miR-486 mimic-NC; b. Mimic group: PMVEC cells were treated with 200 μM $CoCl_2$ for 12 h, followed by transfection of 15 nM miR-486 mimic; c. Inhibitor-NC group: PMVEC cells were treated with 200 μM $CoCl_2$ for 12 h, followed by transfection of 15 nM miR-486 inhibitor-NC; d. Inhibitor group: PMVEC cells were treated with 200 μM $CoCl_2$ for 12 h, followed by transfection of 15 nM miR-486 inhibitor. miR-486 mimic, inhibitor and corresponding negative control (NC) were obtained from Tsingke (Beijing, China), and transfection was conducted using the RNA TransMate reagent (E607402, Sangon Biotech, Shanghai, China).

To verify the role of miRNA-486 on HAPE is linked to the activation of the PI3K/AKT signaling pathway, PMVEC cells were divided into four groups: a. PMVEC cells were treated with 200 μM $CoCl_2$ for 12 h, followed by transfection of 15 nM miR-486 mimic-NC; b. Mimic-NC + Ly294002 group: PMVEC cells were treated with 200 μM $CoCl_2$ for 12 h, followed by treatment with 20 μM PI3K inhibitor Ly294002 (HY-10108, MCE, Shanghai, China) for 30 min, and then transfected with 15 nM miR-486 mimic-NC; c. Mimic group: PMVEC cells were treated with 200 μM $CoCl_2$ for 12 h, followed by transfection of 15 nM miR-486 mimic; d. Mimic + Ly294002 group: PMVEC cells were treated with 200 μM $CoCl_2$ for 12 h, followed by treatment with 20 μM PI3K inhibitor Ly294002 (HY-10108, MCE, Shanghai, China) for 30 min, and then transfected with 15 nM miR-486 mimic.

2.4. Ethics statement for in vivo studies

All procedures involving animals were conducted in strict accordance with the guidelines for the care and use of laboratory animals established by the National Institutes of Health. The Animal Care and Use Committee of the Laboratory Animal Center provided ethical approval for the experimental protocols (IACUC-DWZX-2021-714), ensuring the commitment to the welfare and ethical treatment of the animals involved in the study.

2.5. Rats HAPE model and grouping

Adult Male Sprague-Dawley rats, weighing between 180 and 200 g, were acquired from Beijing Vital River Laboratory Animal Technology Co., Ltd. in Beijing,

Rats were housed in a controlled environment under a 12 h light/dark cycle, with controlled humidity ranging from 50 to 60 % and a stable temperature (22 ± 2 °C). Rats had free access to standard maintenance pelleted food and water ad libitum. To assess the impact of sEVmiR-486 on HAPE, we randomly assigned rats into four groups (n = 7) after 1-week acclimatization: (1) a low-altitude control group (Control) received 100 μl of PBS via the tail vein on days 1 and 3 of hypoxia exposure; (2) an HAPE group (HAPE) received an identical PBS treatment to the control; (3) an sEV^{Null} group (sEV^{Null}) received 1×10^{10} particles/100 μl of sEV^{Null} via the tail vein on the same days; and (4) an $sEV^{miR-486}$ group ($sEV^{miR-486}$) was administered 1×10^{10} particles/100 μl of $sEV^{miR-486}$ via the tail vein also on days 1 and 3 of hypoxic treatment. The dose of sEVs was confirmed based on the results of the preliminary experiment.

All animal subjects, except for the low-altitude control group, underwent acute hypoxic exposure using a simulation chamber (Aebell, China), designed to mimic high-altitude conditions equivalent to 6000 m. The ascent to the simulated altitude was achieved at a controlled rate of 4 m per second.

2.6. Rat cardiac ultrasound

Rats were anesthetized using isoflurane inhalation and positioned supine with limbs secured on the operating table of the instrument. Their chest fur was shaved in preparation for imaging. Cardiac ultrasounds were performed with a Vevo 3100 LT small animal ultrasound imaging system (probe M250, VisualSonics, Toronto, Canada). The system measured pulmonary acceleration time (PAT) and pulmonary ejection time (PET) and used these metrics to derive pulmonary artery pressure (PAP).

2.7. Tissue samples collection

Rats were anesthetized using sodium pentobarbital (40 mg/kg) through intraperitoneal injection at the end of the study. 3 rats per group followed by an abdominal incision to collect blood from the major abdominal vein for hematological and cytokine analyses. The left lung was sampled to assess lung water content, while the right lung was preserved at −80 °C to prepare tissue homogenate and extract RNA. Another 4 rats per group were surgically exposed thoracic cavity, and a cannula was placed into the trachea. The left lung was clamped using hemostatic forceps, after which bronchoalveolar lavage fluid (BALF) was obtained by irrigating the right lung thrice with sterile saline. Subsequently, the left lung tissue was preserved in 4 % paraformaldehyde in preparation for hematoxylin and eosin (H&E) staining.

2.8. Preparation of lung tissue homogenates and BALF

To prepare the lung tissue homogenates, the lower lobe of the right lung was excised and thoroughly homogenized with pre-cooled saline at a 1:9 mass-to-volume ratio. This mixture was then incubated at 4 °C for 30 min followed by centrifugation at 10,000 rpm for 10 min at 4 °C using a refrigerated centrifuge. The supernatant was subsequently collected to yield the final lung tissue homogenate.

The alveolar lavage fluid was obtained by centrifuging the collected BALF at 3000 g for 10 min at 4 °C, followed by careful collection of the resulting supernatant.

2.9. HE staining and immunofluorescence detection

The left lung tissues, which had been fixed, were subsequently embedded in paraffin and sectioned into slices 5 μm in thickness.

Histological alterations in lung tissue were determined via HE staining, while the status of local tight junctions was investigated using immunofluorescence. Tissue sections were covered with fluorescent sealer (BD-FM-1; BDHM, Beijing, China) and incubated at room temperature for 1 h. Subsequently, sections were incubated with anti-Occludin antibody (27260-1-AP; Proteintech, IL, USA) overnight at 4 °C. Following two times of PBS washes, sections were stained using the Opal 520 reagent pack (BD52100; BDHM, Beijing, China). DAPI (BD-DAPI-1; BDHM, Beijing, China) was applied as a counterstain to visualize nuclei.

2.10. Total protein detection

The protein concentrations in both BALF and lung tissue homogenates were quantified using the Pierce™ BCA Protein Assay Kit (Thermo Fisher Scientific, Illinois, USA).

2.11. Rat lung water content(LWC)

Pulmonary edema severity can be gauged by lung water content (LWC). The excised left lung was promptly weighed to obtain the wet weight before being dehydrated at 60 °C for 96 h in an oven until a constant mass was achieved, indicating the dry weight. LWC was calculated using the formula: (wet weight - dry weight)/wet weight.

2.12. Active substances detection

The levels and activity of pertinent bioactive molecules associated with inflammation, oxidative stress, vascular function, and membrane permeability were quantified in serum, plasma, and lung tissue homogenates using rat-specific assay kits as per the manufacturer's protocols, detailed in Table 1.

Table 1
The assay kits used in this study.

Product	Manufacturer	Catalogue Number	Sample
Nitric Oxide (NO) Colorimetric Assay Kit	Elabscience, Wuhan, China	E-BC-K035-M	plasma
PGI2 (Prostacyclin) ELISA Kit		E-EL-0022c	plasma
Rat ET-1(Endothelin 1) ELISA Kit		E-EL-R1458c	plasma
TXA2 (Thromboxane A2) ELISA Kit		E-EL-0057C	plasma
Total Superoxide Dismutase (T-SOD) Activity Assay Kit (WST-1 Method)		E-BC-K020-M	Lung tissue homogenate
Malondialdehyde (MDA) Colorimetric Assay Kit (TBA Method)		E-BC-K025-M	Lung tissue homogenate
Rat IL-6 ELISA Kit	ABclonal, Wuhan, China	RK00020	Lung tissue homogenate
Rat IL-1β ELISA Kit		RK00009	Lung tissue homogenate
Rat Interleukin 1β (IL-1β) ELISA Kit	MEIKE, Jiangsu China	MK1588A	Serum
Rat Interleukin 4 (IL-4) ELISA Kit		MK6742A	Serum
Rat Interleukin 6 (IL-6) ELISA Kit		MK1731A	Serum
Rat Interleukin 10 (IL-10) ELISA Kit		MK1736A	Serum
Rat Interleukin 12 (IL-12) ELISA Kit		MK1681A	Serum
Rat Interleukin 17A (IL-17A) ELISA Kit		MK7071A	Serum
Rat Tumor Necrosis Factor alpha (TNF-α) ELISA Kit		MK1721A	Serum

2.13. Western blot analysis

Lung tissues and PMEVC cells were lysed with RIPA buffer (Epizyme, PC101, China) supplemented with both protease (Epizyme, GRF101, China) and phosphatase inhibitors (Epizyme, GRF102). The lysates underwent centrifugation at 12,000g and 4 °C for 15 min to eliminate cellular debris. Protein concentrations were measured using a UV spectrophotometer (Thermo, IL, USA). Samples containing 10 μg of protein were resolved by polyacrylamide gel electrophoresis and subsequently transferred onto polyvinylidene fluoride (PVDF) membranes. These membranes were blocked and incubated with primary antibodies overnight at 4 °C. Following four washes in Tris-buffered saline with Tween-20 (TBST) of 5 min each, the membranes were incubated with HRP-conjugated secondary antibodies for 1 h at room temperature (RT). We utilized Electrochemiluminescence (ECL) substrate (Zomanbio, Beijing, China) for signal detection and the Tanon imaging system (Tanon, Shanghai, China) for capturing images. A comprehensive list of the antibodies used and the dilution ratio is presented in Table 2.

2.14. Real-time quantitative PCR (qPCR)

Total RNA was isolated from lung tissues and PMVEC using the RNA-Quick Purification Kit (ES Science, Beijing, China) in accordance with the manufacturer's protocol. cDNA synthesis was performed with the Evo M-MLV RT Mix Kit (Acclurate, Hunan, China) for subsequent qPCR assays. The qPCR analyses were carried out with the qPCR SYBR Green I Master kit (Yeasen, Shanghai, China) on the CFX Connect real-time PCR system (Bio-Rad, CA, USA). Each qPCR reaction was executed in quadruplicate. Relative gene expression levels were calculated using the $2^{-\Delta\Delta Ct}$ method, normalizing against β-actin as the internal control. Primer sequences employed in the study are detailed in Table 3.

2.15. Flow cytometry

Reactive oxygen species (ROS) working solutions, provided by Byotime (Shanghai, China), were prepared following the manufacturer's instructions. The cells were incubated with the ROS working solution for 20 min at 37 °C, and then washed with serum-free cell culture medium for three times. Subsequently, the ROS signal was detected using fluorescence-activated cell sorting (FACS; BD, NJ, USA). The mean fluorescence intensity of ROS was quantified using FlowJo software.

2.16. miRNA Sequencing of sEV^{Null} and $sEV^{miR-486}$

Total RNA from sEV^{Null} and $sEV^{miR-486}$ was extracted for miRNA sequencing. Differentially expressed miRNAs underwent analysis with the online Dr. TOM software (BGI-Shenzhen, China) for gene ontology and pathway enrichment.

2.17. Statistical

All experiments were conducted a minimum of three times, with results presented as the mean ± standard deviation (SD). Statistical evaluation was carried out via GraphPad Prism 9, employing one-way ANOVA for analyses across multiple groups and unpaired t-tests for bipartite comparisons. $P < 0.05$ was considered of statistical significance.

Table 2
Primary and secondary antibodies used in this study.

Product	Cat. No.	Dilution ratio	Company
Anti-Aquaporin 5 antibody	ab78486	1:10000	Abcam, USA
Anti-Aquaporin 1 antibody	ab168387	1:5000	
Anti-Heme Oxygenase 1 antibody	ab68477	1:1000	
Anti-Occludin antibody	ab167161	1:1000	
Anti-TSG101 antibody	ab125011	1:1000	
Anti-CD63 antibody	ab134045	1:1000	
Anti-CD9 antibody	ab236630	1:1000	
Anti-beta III Tubulin antibody	ab18207	1:10000	
Anti-eNOS antibody	ab5589	1:1000	
NRF2(E3J1V) Rabbit mAb	33649	1:1000	Cell Signaling, USA
Keap1 (D6B12) Rabbit mAb	8047S	1:1000	
PI3 kinase P85 Rabbit	4257T	1:1000	
Phospho-Akt (Ser473) Rabbit mAb	4060S	1:2000	
Thy1/CD90 (D3V8A) Rabbit mAb	13801S	1:1000	
Akt antibody	9272S	1:1000	
TRPV4 antibody	DF8624	1:3000	Affbiotech, China
ZO-1 antibody	AF5145	1:1000	
beta Actin Rabbit pAb	380624	1:10000	ZENBIO, China
Goat Anti-rabbitt IgG (H + L)	BST18D06A8E54	1:5000	Boster, China

Table 3
Primer sequence used in this study.

Gene	Sequences (5′–3′)
β-actin (Rat)	Forward: CACCCGCGAGTACAACCTTC Reverse: CCCATACCCACCATCACACC
AQP-1(Rat)	Forward: CTGGCCTTTGGTTTGAGCAT Reverse: CCACACACTGGGCGATGAT
AQP-5 (Rat)	Forward: GCCACATCAATCCAGCCATT Reverse: AAAGATCGGGCTGGGTTGAT
PTEN (Rat)	Forward: GGGAAAGGACGGACTGGTGT Reverse: ATAGCGCCTCTGACTGGGAAT
AKT1 (Rat)	Forward: ACCACCGCCATTCAGACTG -3′ Reverse: TTGTCACTGGGTGAACCTGA
PDK1 (Rat)	Forward: GAACTGTTCAAGAACGCAATGA Reverse: CCAGTGTGACGTGAACTTGAAT
NOS3 (Rat)	Forward: GAGCAGCACAAGAGTTACAAAATCC Reverse: TCCACCGCTCGAGCAAAG
SOD2 (Rat)	Forward: ATTAACGCGCAGATCATGCA Reverse: CCTCGGTGACGTTCAGATTGT
CAT (Rat)	Forward: CGTCACTCAGGTGCGGACATTC Reverse: TCAGGTGGTTGGCAATGTTCTCAC
Na^+K^+-ATPase (Rat)	Forward: CTGATCAGCATGGCCTATGGAC Reverse: ACCGTTCTCAGCCAGAATCACA
MiR-486 (Human)	Forward: CTCTGATCTCGCCCTCCCT Reverse: CTTGTTCCCCGTTGTCTCCC
U6 (Human)	Forward: CTCGCTTCGGCAGCACA Reverse: AACGCTTCACGAATTTGCGT

3. Results

3.1. Isolation and identification of sEVs

sEVs were isolated via differential ultracentrifugation, and nanoparticle tracking analysis indicated a size distribution ranging from 70 to 150 nm, with a predominant diameter of 136 nm (Fig. 1A). The transmission electron microscopy (TEM) images revealed that the sEVs possessed a rounded morphology and a bilayer membrane structure, measuring approximately 100 nm in diameter (Fig. 1B).

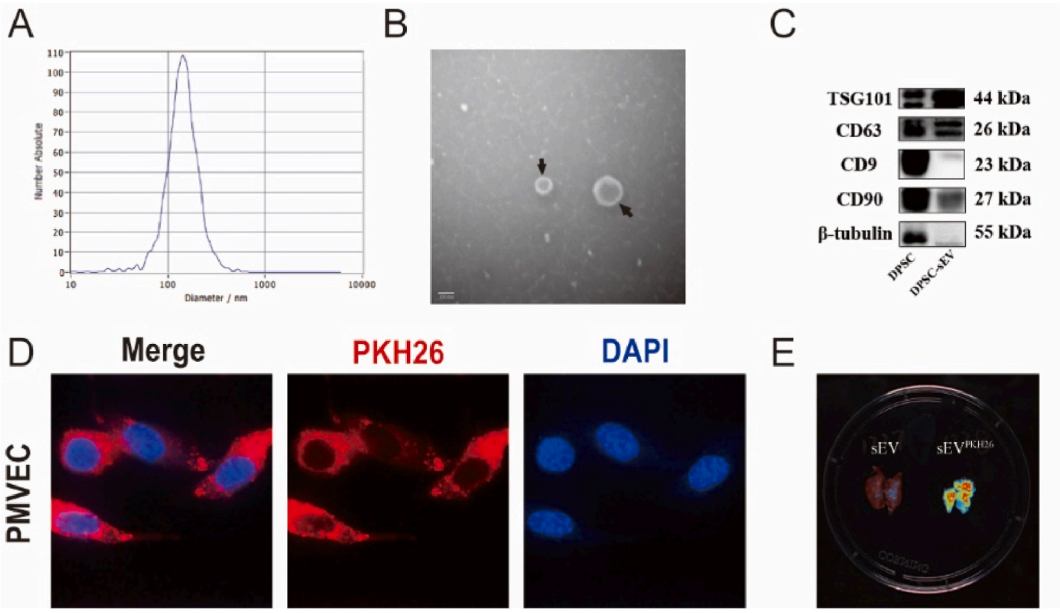

Fig. 1. Isolation and identification of sEVs. (A) Depicts nanoparticle tracking analysis employed to ascertain the particle size distribution of sEVs. (B) Shows the application of transmission electron microscopy in visualizing the structure and size of sEVs with a scale bar denoting 100 nm. (C) Illustrates the utilization of Western blotting to detect the hallmark proteins of sEVs. (D) Demonstrates the uptake of sEVs by PMVEC, as captured by a confocal fluorescence microscope with a scale bar of 10 μm. (E) Presents in vivo imaging techniques to monitor the sEVs penetration into mouse lung tissue.

Further, Western blot analysis confirmed the presence of established sEVs markers Tsg101, CD63, and CD9, as well as CD90, a signature protein of DPSCs (Fig. 1C). To assess cellular uptake, PKH26-labeled sEVs were incubated with PMVEC. Fluorescence microscopy performed 24 h post-co-culture showed successful internalization of sEVs by PMVEC (Fig. 1D). Additionally, systemic distribution was examined by injecting PKH26-stained sEVs through the tail vein of mice; subsequent in vivo optical imaging with Xenogen revealed prominent fluorescence in the lungs 24 h after injection (Fig. 1E). Collectively, these findings substantiate that the purified sEVs conform to the characteristics of sEVs and are capable of entering both cellular and pulmonary tissue.

3.2. $sEV^{miR-486}$ repair the damaged lung tissue in HAPE rat model

To enhance therapeutic outcomes, we treated DPSCs with Ad.miR-486 to produce sEVs that overexpress miR-486. Quantitative PCR analysis confirmed a significant increase in miR-486 expression in DPSCs transduced with Ad.miR-486 (Fig. 2A). Small RNA sequencing demonstrated a substantial enrichment of miR-486 within $sEV^{miR-486}$ compared to sEV^{Null} (Fig. 2B). We then assessed the therapeutic impact of $sEV^{miR-486}$ on HAPE by administering sEV^{Null} and $sEV^{miR-486}$ to HAPE afflicted rats and monitoring pulmonary arterial pressure via a small animal ultrasound imaging system. The results indicated a significant reduction in the elevated pressure post-treatment (Fig. 2C and D). The results of HE staining of lung tissues showed destroyed alveolar structure, alveolar wall thickening, alveolar and interstitial edema, alveolar hemorrhage, and increased inflammatory infiltration in HAPE rats, whereas those treated with sEV^{Null} and $sEV^{miR-486}$ could alleviate these pathological manifestations mediated by hypobaric hypoxia (Fig. 2E). Moreover, lung water content a marker of pulmonary edema was significantly reduced following treatment (Fig. 2F), suggesting edema amelioration. The bicinchoninic acid assay indicated that sEV^{Null} and $sEV^{miR-486}$ treatments significantly lowered the protein content in lung homogenates and bronchoalveolar lavage fluid, reflecting restored lung tissue permeability; the $sEV^{miR-486}$ group showed a statistically significant improvement over the sEV^{Null} group (Fig. 2G). Collectively, our study indicates that sEVs overexpressing miR-486 can mitigate pulmonary arterial pressure elevation, reduce alveolar damage, and improve lung permeability in HAPE, with $sEV^{miR-486}$ demonstrating superior histopathological amelioration relative to sEV^{Null}.

3.3. $sEV^{miR-486}$ mitigates lung injury by modulating oxidative stress and inflammation

To preliminarily investigate the reparative mechanism of $sEV^{miR-486}$ on HAPE, we assessed the expression of oxidative stress and inflammation-related factors. Notably, SOD specific activity was found to be decreased, while MDA levels were increased in lung tissue homogenates of the HAPE group compared to controls; these alterations were mitigated by sEV^{Null} and $sEV^{miR-486}$ treatments, with the latter exhibiting a more pronounced effect (Fig. 3A). Similarly, expression changes in oxidative stress-related genes were observed in hypoxia-injured PMVEC, where SOD2 expression declined and Catalase (CAT) expression rose following hypoxic injury, yet both were ameliorated following treatment with sEV^{Null} and $sEV^{miR-486}$. Notably, there was a significant difference in SOD2 expression between the sEV^{Null} and $sEV^{miR-486}$ groups (Fig. 3B), suggesting that $sEV^{miR-486}$ may enhance PMVEC resistance to oxidative stress. Furthermore, we examined key protein expressions in the Nrf2/keap1/HO-1 pathway via Western blot and observed that hypoxic injury intensified the intracellular degradation of Nrf2 and Keap1, and diminished HO-1 expression. Contrastingly, cells treated with

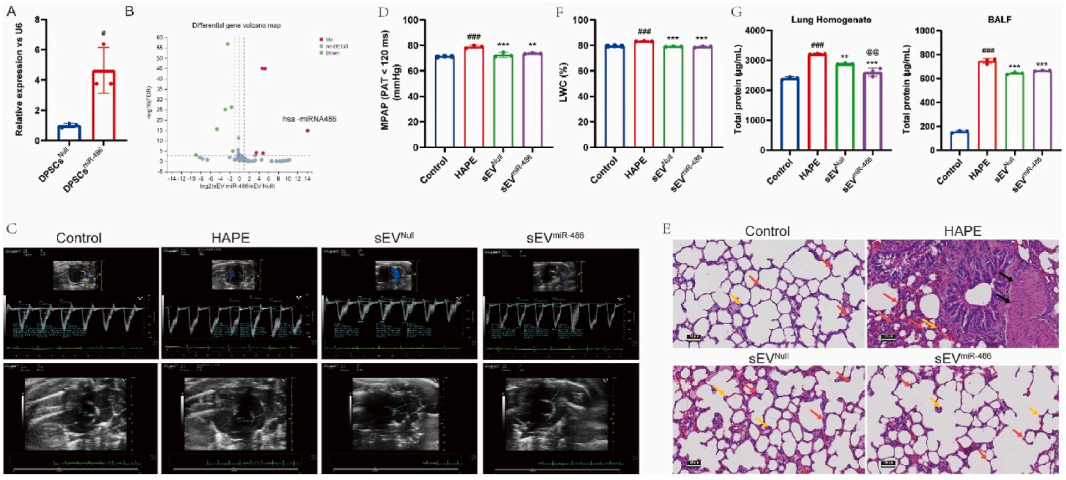

Fig. 2. $sEV^{miR-486}$ repair the damaged lung tissue in HAPE rat model (A) Expression of miR-486 in DPSCs following infection with Ad.Null or Ad.miR-486. (B) A volcano plot illustrating differentially expressed small RNA between sEV^{Null} and $sEV^{miR-486}$ treatments. (C) Cardiac ultrasound images accompanied by (D) a statistical histogram quantifying the results. (E) Hematoxylin and eosin (HE) stained sections of lung tissue; alveolar walls are marked by red arrows, smooth muscle by black arrows, and alveolar septa by yellow arrows. (F) Measurement of water content in rat lung tissue. (G) Quantification of protein levels in lung tissue homogenates and bronchoalveolar lavage fluid. Images are annotated with a scale bar representing 50 μm. Data represent means ± SD. Statistical significance is indicated as follows: $^{\#}p < 0.05$, $^{\#\#\#}p < 0.001$, versus the control group; $^{**}p < 0.01$, $^{***}p < 0.001$, versus the HAPE group; $^{@@}p < 0.01$, versus the sEV^{Null} group.

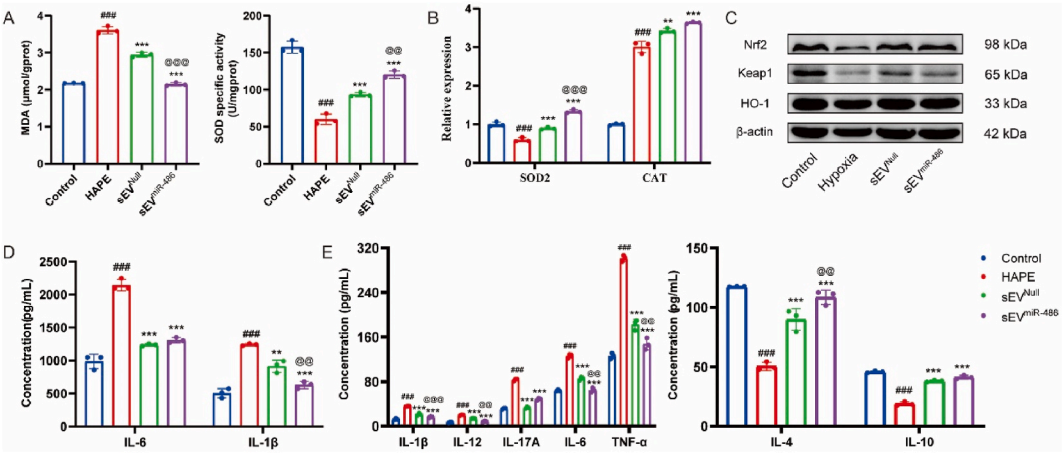

Fig. 3. $sEV^{miR-486}$ mitigates lung injury by modulating oxidative stress and inflammation (A) Presents the concentrations of MDA and the activity of SOD in lung tissue homogenates. (B) Details the gene expression of SOD2 and CAT in PMVEC, as measured by quantitative PCR. (C)The protein expression levels of Nrf2, keap1, and HO-1 in PMVEC were revealed through Western blot analysis. (D) ELISA was used to detect the expression levels of IL-1β and IL-6 in the lung tissue homogenates. (E) Depicts the serum concentrations of a spectrum of cytokines—IL-1β, IL-6, IL-12, IL-17A, TNF-α, IL-4, and IL-10 quantified via ELISA. Data are expressed as means ± SD. Statistical significance is denoted by $^{\#\#\#}p < 0.001$ compared with the control group; $^{**}p < 0.01$, $^{***}p < 0.001$ compared with the HAPE group or the hypoxia group; $^{@@}p < 0.01$, $^{@@@}p < 0.001$, compared with sEV^{Null} group.

sEV^{Null} and $sEV^{miR-486}$ displayed significantly higher levels of total Nrf2, Keap1, and HO-1 expression (Fig. 3C).

Inflammation is crucial to the onset and progression of HAPE. We assessed the levels of inflammation-related cytokines in lung tissue homogenates and serum. Our findings revealed that, relative to the control group, levels of pro-inflammatory cytokines IL-1β and IL-6 were elevated in lung tissue homogenates (Fig. 3D). Moreover, serum concentrations of pro-inflammatory cytokines IL-1β, IL-6, IL-12, IL-17A, and TNF-α significantly increased, while the anti-inflammatory cytokines IL-4 and IL-10 were reduced in the HAPE group (Fig. 3E). Treatments with sEV^{Null} and $sEV^{miR-486}$ partially mitigated these alterations in cytokine expression induced by low pressure and hypoxia, with the $sEV^{miR-486}$ group demonstrating a more marked effect than the sEV^{Null} group (Fig. 3D and E). In conclusion, both sEV^{Null} and $sEV^{miR-486}$ treatments were effective in attenuating HAPE-induced lung injury by modulating oxidative stress and inflammation, with $sEV^{miR-486}$ showing superior efficacy.

3.4. *$sEV^{miR-486}$ ameliorates lung injury by restoring intercellular tight junctions and permeability*

Exposure to low pressure and hypoxia often compromises tight junction integrity and exacerbates hypoxic pulmonary vasoconstriction (HPV). We also assessed the expression of tight junction proteins, vasoactive mediators, and cell permeability markers. Immunofluorescence staining revealed a substantial reduction in tight junction protein Occludin in the lung tissues of rats with HAPE compared to controls, while sEV^{Null} and $sEV^{miR-486}$ treatment significantly restored Occludin expression (Fig. 4A). Western blot analysis demonstrated similar effects for ZO-1 and Occludin in PMVECs post hypoxic injury (Fig. 4B). ELISA of rat plasma indicated that ET-1 and TXA2 levels were significantly elevated while NO and PGI2 were reduced following hypoxia; these alterations were partially mitigated by sEV^{Null} and $sEV^{miR-486}$, with a more marked improvement observed in the $sEV^{miR-486}$ treated group (Fig. 4C). qPCR on rat lung tissues highlighted a decrease in aquaporins AQP-1 and AQP-5 in HAPE, which were upregulated following sEV treatments (Fig. 4D). Additionally, qPCR and Western blot analyses showed a significant downregulation in AQP-1, AQP-5, and Na^+/K^+-ATPase, alongside an upregulation in TRPV4 in hypoxia-injured PMVEC, changes that were partially reversed by sEV treatments, especially with $sEV^{miR-486}$ (Fig. 4E). These results align with those observed in HAPE rat models. In conclusion, sEV^{Null} and $sEV^{miR-486}$ can mitigate HAPE and hypoxia-induced injuries by modulating intercellular tight junctions, vasoactive factors, and cellular permeability, with $sEV^{miR-486}$ showing superior efficacy.

3.5. *miR-486 reduces oxidative stress by regulating the PTEN/PI3K/Akt/eNOS signaling pathway*

To elucidate the role of miR-486 in modulating hypoxia-induced lung injury, we conducted a KEGG enrichment analysis on the miRNA expression profiles in sEV^{Null} and $sEV^{miR-486}$. We discovered an enrichment of the PI3K-Akt signaling pathway within the differential miRNAs of both variants (Fig. 5A). The PTEN was identified as target gene of miR-486 in our previous study [26]. Considering PTEN's regulatory role in Akt synthesis within the PI3K-Akt pathway, we assessed PTEN and Akt1 expression via qPCR. The results indicated a marked reduction in PTEN and a concomitant increase in Akt1 expression following treatment with sEV^{Null} and $sEV^{miR-486}$; notably, the latter had a more pronounced effect (Fig. 5B). Within this pathway, Akt has been noted to augment eNOS expression and enhance NO secretion through phosphorylation. Hence, we examined the expression of the NOS3 gene and eNOS protein by qPCR and Western blot, respectively. Following hypoxic damage in PMVEC cells, there was a decrease in NOS3 mRNA and

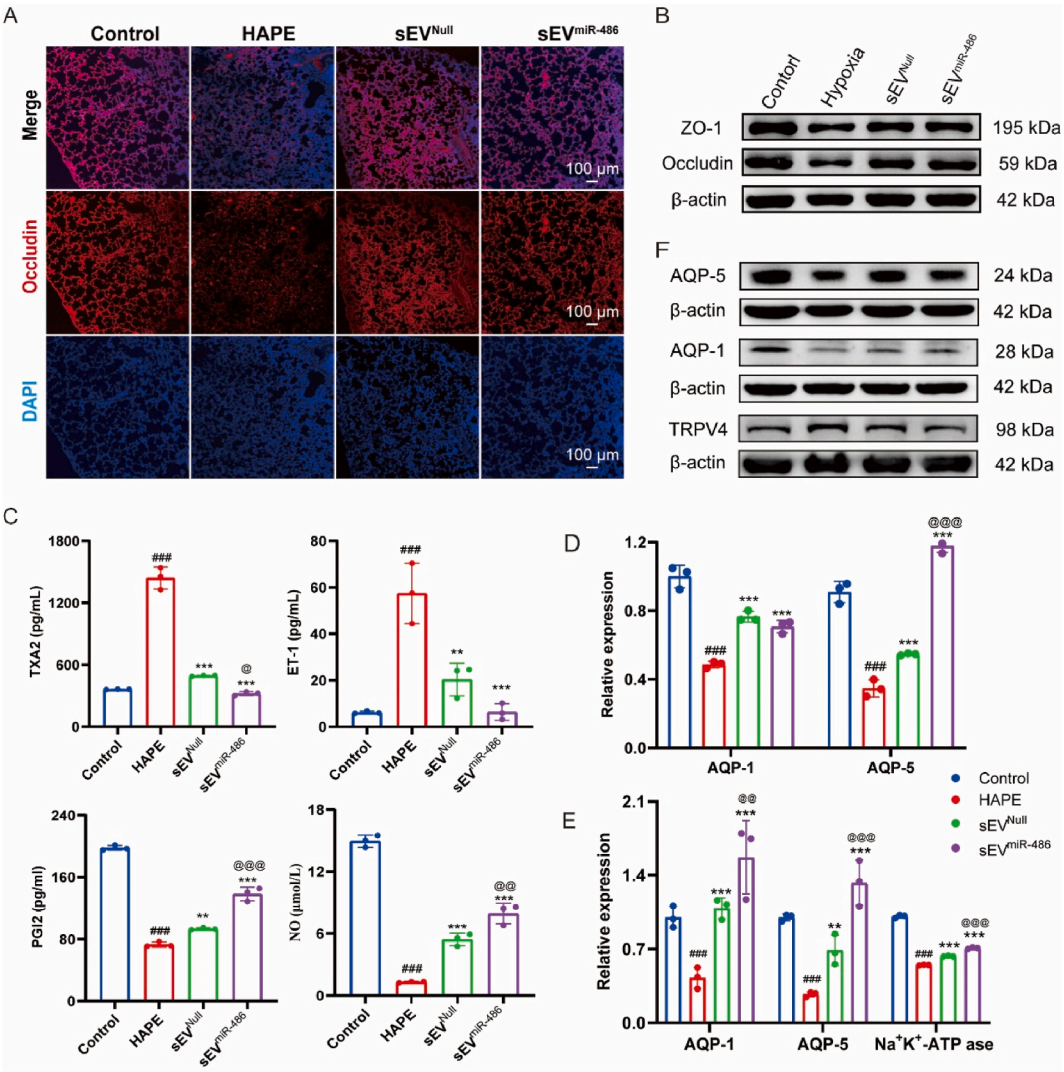

Fig. 4. $sEV^{miR-486}$ ameliorates lung injury by restoring intercellular tight junctions and permeability (A) Exhibits representative immunofluorescence images of Occludin protein levels in rat lung tissue. (B) Assesses the expression of tight junction proteins ZO-1 and Occludin in PMVEC using Western blot analysis. (C) Employs ELISA to measure plasma concentrations of TXA2, ET-1, NO, and PGI2 in rats. Moreover. (D) Quantifies mRNA levels of permeability-associated genes AQP-1 and AQP-5 in rat lung tissues via quantitative PCR. (E) Reports the corresponding mRNA levels in PMVEC. (F) Presents the protein expression levels of TRPV4, AQP-1, and AQP-5 in PMVEC. Data are expressed as means ± SD. Statistical significance is denoted as follows: $^{###}p < 0.001$ versus the control group; $^{**}p < 0.01$, $^{***}p < 0.001$ versus the HAPE or hypoxia groups; $^{@}p < 0.05$, $^{@@}p < 0.01$, $^{@@@}p < 0.001$ versus the sEV^{Null} group.

eNOS protein levels. However, treatment with sEV^{Null} and $sEV^{miR-486}$ reversed this effect, elevating the expression levels of NOS3 and eNOS, with $sEV^{miR-486}$ having a more pronounced impact (Fig. 5C and D).

To further investigate the regulatory influence of miR-486 on the PI3K-Akt signaling pathway, we transfected PMVEC cells with miR-486 mimic and inhibitor. Transfection with the mimic yielded a marked increase in miR-486 expression, whereas the inhibitor led to a reduction (Fig. 5E). Transfection with the miR-486 mimic downregulated PTEN gene expression and upregulated Akt1 and PDK1 expression in PMVECs. Conversely, the miR-486 inhibitor induced an increase in PTEN expression and a decrease in Akt1 and PDK1 expression (Fig. 5F). Western blot analysis further confirmed that transfection with miR-486 mimic increased the expression levels of p-Akt, PI3K, and eNOS, while the inhibitor reduced their expression (Fig. 5G). To elucidate the role of miR-486 in modulating oxidative stress via the PI3K-Akt pathway, we assessed ROS levels in PMVEC cells by flow cytometry. The findings demonstrate a decrease in ROS levels following miR-486 mimic transfection and a significant increase after inhibitor transfection (Fig. 5H). Furthermore, to verify the role of miRNA-486 on HAPE is linked to the activation of the PI3K/AKT signaling pathway, we used the PI3K inhibitor Ly294002 to evaluate the effect of PI3K blockade on oxidative stress in PMVEC cells induced by hypoxia. ROS levels of PMVEC cells were detected by using flow cytometry, and the results demonstrated that the antioxidant effect of the miR-486 mimic was partially suppressed by Ly294002 (Fig. 5I).

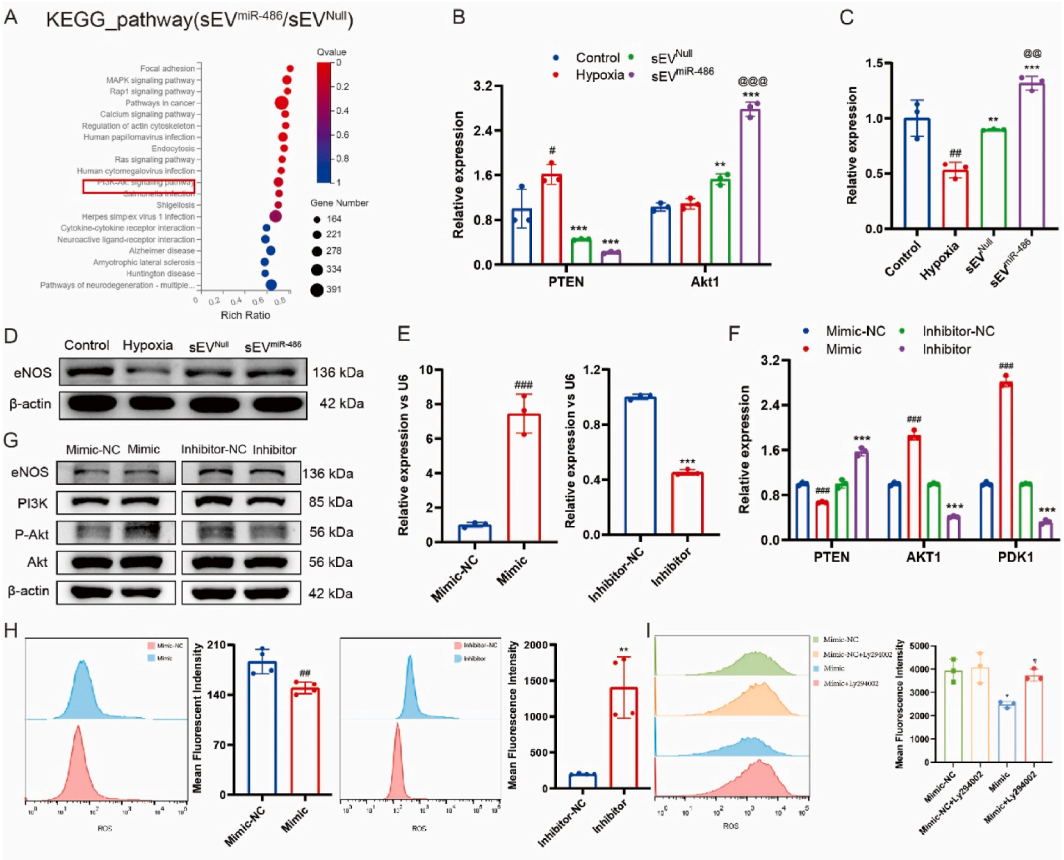

Fig. 5. miR-486 reduces oxidative stress by regulating the PTEN/PI3K/Akt/eNOS signaling pathway (A) A KEGG analysis identifies differentially expressed genes between sEV^{Null} and $sEV^{miR-486}$. (B) The mRNA levels of PTEN and Akt1 in PMVEC cells were quantified by qPCR. (C) NOS3 mRNA expression in PMVEC cells was assessed using qPCR. (D) The protein level of eNOS in PMVEC cells was evaluated by Western blot. Statistically significant differences are denoted by the following: $^{\#}p < 0.05$ and $^{\#\#}p < 0.01$ against the control group; $^{**}p < 0.01$ and $^{***}p < 0.001$ versus the hypoxia group; $^{@@}p < 0.01$ and $^{@@@}p < 0.001$ in comparison to the sEV^{Null} group. (E) qPCR was employed to measure the expression of miR-486 in PMVEC cells following transfection with either a miR-486 mimic or inhibitor. (F) Expressions of PTEN, Akt1, and PDK1 genes in PMVEC cells post-transfection were quantified by qPCR. (G) A phosphorylated protein Western blot analysis determined the levels of Akt1, p-Akt1, PI3K, and eNOS in PMVEC cells transfected with miR-486 mimic or inhibitor. (H) Flow cytometry was utilized to examine the ROS production in PMVEC cells following transfection. $^{\#\#\#}p < 0.001$, versus the Mimic-NC group; $^{***}p < 0.001$, versus the Inhibitor-NC group. (I)Flow cytometry was used to detect the ROS production in PMVEC cells after Ly294002 was used to inhibit the PI3K signaling. $^{*}p < 0.05$, versus the Mimic-NC group. $^{\#}p < 0.05$, versus the Mimic group. Data are expressed as means ± SD.

Collectively, these results suggest that miR-486 may mitigate hypoxia-induced oxidative stress in PMVEC cells through modulation of the PI3K/Akt signaling pathway.

4. Discussion

In this study, we explored the therapeutic potential of sEV^{Null} and $sEV^{miR-486}$ for HAPE. Our results demonstrate that sEV^{Null} and $sEV^{miR-486}$ mitigate pulmonary hypertension and edema in HAPE afflicted rats by modulating oxidative stress, inflammation, vascular reactivity, lung tissue permeability, and the integrity of intercellular tight junctions via the Nrf2/keap1/HO-1/eNOS pathway. Additionally, $sEV^{miR-486}$ was found to further suppress oxidative stress through the PI3K-Akt signaling pathway, thereby exerting a more pronounced therapeutic effect. A schematic of these putative therapeutic mechanisms is depicted in Fig. 6 (Figdraw, RSOURe189e).

HAPE manifests as noncardiogenic pulmonary edema characterized by hypoxic pulmonary hypertension, heightened alveolar capillary membrane permeability, and alveolar congestion [28,29]. Present pharmacologic interventions for HAPE, such as glucocorticoids, pulmonary vasodilators, and carbonic anhydrase inhibitors, exhibit restricted therapeutic efficacy and are associated with notable adverse effects [30]. Consequently, there is an imperative need to identify a therapeutic regimen that is both safe and effective.

In studies utilizing rat models designed to emulate HAPE, researchers observed that reduced pressure and hypoxic conditions augmented endothelial permeability within lung tissues. This alteration led to heightened total protein levels in BALF, precipitating

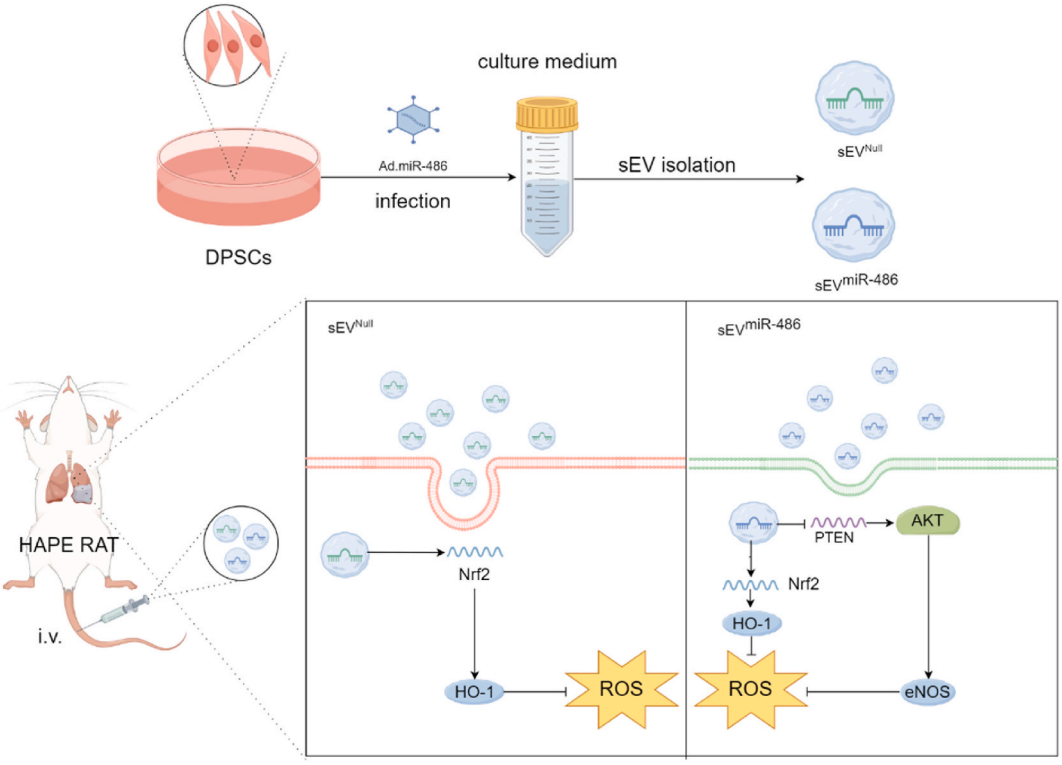

Fig. 6. Schematic diagram showing the effects of small extracellular vesicles derived from miRNA-486 overexpressed dental pulp stem cells on HAPE.

pulmonary edema and subsequent elevated release of inflammatory cytokines including IL-1β and IL-6 [31,32]. In our investigation, we successfully established a rat HAPE model employing a high-altitude environmental simulation chamber. Our observations revealed enhanced permeability of lung tissues coupled with a significant upregulation in the expression of inflammatory mediators.

MSCs have been reported to mitigate acute lung injury-induced pulmonary edema, modulate immune responses, and attenuate inflammation via paracrine effects [33]. Subsequent research has demonstrated that MSC-sEV could improve pulmonary vascular integrity post-hemorrhagic shock and ameliorate ischemia/reperfusion-induced pulmonary edema and inflammation [34,35]. In the present study, DPSC-sEVs were chosen to investigate the effects of miR-486 overexpression on HAPE. By infecting DPSCs with Ad. miR-486 to yield DPSC-sEVs with elevated levels of miR-486 ($sEV^{miR-486}$), we intended to potentiate the therapeutic benefits of DPSC-sEVs. Our findings suggest that $sEV^{miR-486}$ significantly decreased pulmonary artery pressure, reduced pulmonary edema, and improved lung tissue permeability and damage more effectively than sEV^{Null}, likely by diminishing oxidative stress and inflammation.

Exposure to low-pressure hypoxia has been associated with increased oxidative stress biomarkers, with studies demonstrating that oxidative stress is rapidly induced in the lungs at high altitudes [36]. Notably, levels of ROS and MDA, a well-known oxidative stress marker, rise in rat lungs within 1.5 h of acute hypoxic exposure [5]. ROS accumulation is linked to the development of HAPE [37]. Our investigation involved measuring MDA concentration and SOD activity in lung tissue homogenates of rats. The findings indicated that high-altitude hypoxia resulted in elevated MDA levels and reduced SOD activity, exacerbating oxidative stress in HAPE-affected rats. Treatment with sEV^{Null} and $sEV^{miR-486}$ was found to mitigate oxidative stress, with $sEV^{miR-486}$ exerting a more pronounced protective effect than sEV^{Null}.

Nrf2 is a transcription factor that orchestrates the regulation of numerous antioxidant proteins. Typically, Nrf2 interacts with Keap1 within the cytoplasm and undergoes ubiquitin-proteasome pathway-mediated degradation. In the rat model of HAPE, Nrf2 activation effectively mitigates ROS generation and oxidative stress [38], suggesting that Nrf2 upregulation could attenuate injury induced by high-altitude hypoxia. Our study observed a decrease in the expression of Nrf2, Keap1, and HO-1 after hypoxic injury in PMVEC cells, which was reversed following treatment with both sEV^{Null} and $sEV^{miR-486}$, indicating that these treatments alleviate oxidative stress by modulating the Nrf2/Keap1/HO-1 pathway. Notably, no significant differences were noted between the sEV^{Null} and $sEV^{miR-486}$ groups, leading us to hypothesize the involvement of an alternate pathway by $sEV^{miR-486}$. Consequently, miRNA sequencing revealed significant alterations in the PI3K-Akt signaling pathway between sEV^{Null} and $sEV^{miR-486}$ via KEGG enrichment analysis. PTEN, as a target of miR-486, is known to dampen Akt1 activity through PIP3 dephosphorylation, curtailing Akt phosphorylation and eNOS production, thereby exacerbating oxidative stress. Our findings indicate that $sEV^{miR-486}$ suppresses PTEN expression, augmenting eNOS synthesis and diminishing oxidative stress. Post-hypoxic injury, we detected a decrease in both NOS3 gene expression and eNOS protein levels in PMVEC cells, which were restored upon sEVs treatments, with $sEV^{miR-486}$ exerting a more

potent effect. The utilization of miR-486 mimics and inhibitors further confirmed that miR-486 enhances eNOS production by inhibiting PTEN, thus influencing the PI3K-Akt pathway. Moreover, miR-486 could reduce ROS levels of PMVEC cells compared to controls, signifying the potential of miR-486 to inhibit ROS formation and oxidative stress.

HPV is a fundamental pathological hallmark of HAPE, serving as an evolutionary conserved response to alveolar hypoxia that enhances ventilation-perfusion matching for efficient gas exchange [39]. However, sustained hypoxia can trigger a pathological increase in pulmonary artery pressure and vascular resistance, contributing to HAPE's severe and potentially fatal effects. This pressure surge may arise from a dysregulated balance in vasoconstriction due to heightened sympathetic stimulation via α-adrenergic pathways [40]. Moreover, vasoactive agents such as ET-1, PGI2, NO, and TXA2 are pivotal in the regulation of HPV [41,42]. In addition, these indicators are also closely related to lung endothelial permeability. Endothelial derived PGI2 usually binds to NO and has effective anti-inflammatory and barrier protective effects on pulmonary vascular endothelial cells [43]. ET-1 can up-regulate the overexpression of vascular endothelial growth/permeability factor (VEGF-A), resulting in increased vascular permeability [44]. TXA2 induces endothelial barrier destruction through intracellular Ca^{2+} and Rho kinase [45].Our study demonstrated that decreased levels of NO and PGI2 alongside elevated ET-1 and TXA2 in HAPE rats, indicating intensified vasoconstriction and impeded vasodilation, leading to increased vascular pressure. Treatment with sEVs markedly enhanced concentrations of vasodilatory NO and PGI2 and concurrently diminished ET-1 and TXA2 levels, implying a restoration of vasoreactivity and mitigation of HPV. Notably, the therapeutic potency of $sEV^{miR-486}$ surpassed that of sEV^{Null}, offering a promising intervention against HAPE. In addition, Nrf2/HO-1 is essential for the protection of neuronal structure and function through downregulation of oxidative damage [46]. Can protected peripheral nerves indirectly reduce HPV in turn? Although there is not enough data to support this hypothesis in this study, we will focus on this issue in future research.

Histologic and microscopic analyses of HAPE have uncovered the presence of hyaline membranes, arterial thromboses, pulmonary hemorrhage, bronchial cellular infiltration, damage to alveolar epithelial cells, expanded gaps in pulmonary capillary cell connections, and a compromised air-blood barrier [6]. Previous research indicated that the loss of tight junction proteins among endothelial cells, notably in LPS-induced acute lung injuries, undermines pulmonary vascular integrity, exacerbating edema [47]. We have examined the levels of tight junction proteins, specifically Occludin, in lung tissue via immunofluorescence and measured the expression of Occludin and ZO-1 in PMVEC impaired by hypoxia using Western blotting. The findings reveal that their expression diminishes under both high-altitude and cobalt chloride-induced hypoxia, with subsequent restoration upon treatment with sEV^{Null} and $sEV^{miR-486}$. Notably, $sEV^{miR-486}$ demonstrates a pronounced ability to mitigate endothelial cell damage and preserve the structural integrity of the pulmonary microvascular endothelial barrier.

5. Conclusion

The current study showed the effectiveness of $sEV^{miR-486}$ to mitigate oxidative stress by activating the PI3K/AKT/eNOS signaling pathway in a rat model of HAPE. Furthermore, $sEV^{miR-486}$ contributes to the alleviation of HAPE by dampening inflammatory responses, enhancing intercellular tight junction integrity, and reestablishing cellular permeability. Consequently, $sEV^{miR-486}$ holds promise as an innovative and potent treatment strategy for HAPE.

CRediT authorship contribution statement

Changyao Wang: Writing – original draft, Investigation, Formal analysis, Data curation. **Zhuang Mao:** Investigation, Formal analysis. **Drolma Gomchok:** Investigation, Formal analysis. **Xue Li:** Investigation, Formal analysis. **Huifang Liu:** Investigation, Formal analysis. **Jingyuan Shao:** Investigation, Formal analysis. **Hu Cao:** Investigation, Formal analysis. **Guanzhen Xue:** Investigation, Formal analysis. **Lin Lv:** Investigation, Formal analysis. **Junzhao Duan:** Investigation, Formal analysis. **Tana Wuren:** Resources, Methodology. **Hua Wang:** Writing – review & editing, Supervision, Project administration, Conceptualization.

Ethics approval

The procedures in animal experiments were reviewed and approved by the Animal Care and Use Committee of the Laboratory Animal Center (IACUC-DWZX-2021-714).

Consent for publication

Not applicable.

Availability of data and materials

All data generated or analyzed during this study are included in this published article and its supplementary information files. However, the data that support the findings of this study are available from the corresponding author upon reasonable request.

Funding

Not applicable.

Declaration of competing interest

The authors declare that they have no known competing financial interests or personal relationships that could have appeared to influence the work reported in this paper.

Acknowledgements

We thank Professor Rili Ge and Feng Tang for their assistance in establishing the HAPE model.

Appendix A. Supplementary data

Supplementary data to this article can be found online at https://doi.org/10.1016/j.heliyon.2025.e41960.

References

[1] A.M. Luks, B.A. Beidleman, L. Freer, C.K. Grissom, L.E. Keyes, S.E. McIntosh, G.W. Rodway, R.B. Schoene, K. Zafren, P.H. Hackett, Wilderness medical society clinical practice guidelines for the prevention, diagnosis, and treatment of acute altitude illness: 2024 update, Wilderness Environ. Med. 35 (1_suppl) (2024) 2S–19S, https://doi.org/10.1016/j.wem.2023.05.013.
[2] P.H. Hackett, R.C. Roach, High-altitude illness, N. Engl. J. Med. 345 (2) (2001) 107–114, https://doi.org/10.1056/NEJM200107123450206.
[3] J.O. Stream, C.K. Grissom, Update on high-altitude pulmonary edema: pathogenesis, prevention, and treatment, Wilderness Environ. Med. 19 (4) (2008) 293–303, https://doi.org/10.1580/07-WEME-REV-173.1.
[4] R.B. Schoene, Illnesses at high altitude, Chest 134 (2) (2008) 402–416, https://doi.org/10.1378/chest.07-0561.
[5] S. Sarada, P. Himadri, C. Mishra, P. Geetali, M.S. Ram, G. Ilavazhagan, Role of oxidative stress and NFkB in hypoxia-induced pulmonary edema, Exp. Biol. Med. (Maywood, NJ, U. S.) 233 (9) (2008) 1088–1098, https://doi.org/10.3181/0712-RM-337.
[6] P. Bärtsch, H. Mairbäurl, M. Maggiorini, E.R. Swenson, Physiological aspects of high-altitude pulmonary edema, J. Appl. Physiol. 98 (3) (2005) 1101–1110, https://doi.org/10.1152/japplphysiol.01167.2004.
[7] H. Qin, A. Zhao, Mesenchymal stem cell therapy for acute respiratory distress syndrome: from basic to clinics, Protein & cell 11 (10) (2020) 707–722, https://doi.org/10.1007/s13238-020-00738-2.
[8] B. Liu, F.X. Ding, Y. Liu, G. Xiong, T. Lin, D.W. He, Y.Y. Zhang, D.Y. Zhang, G.H. Wei, Human umbilical cord-derived mesenchymal stem cells conditioned medium attenuate interstitial fibrosis and stimulate the repair of tubular epithelial cells in an irreversible model of unilateral ureteral obstruction, Nephrology 23 (8) (2018) 728–736, https://doi.org/10.1111/nep.13099.
[9] M. Ezquer, C.A. Urzua, S. Montecino, K. Leal, P. Conget, F. Ezquer, Intravitreal administration of multipotent mesenchymal stromal cells triggers a cytoprotective microenvironment in the retina of diabetic mice, Stem Cell Res. Ther. 7 (2016) 42, https://doi.org/10.1186/s13287-016-0299-y.
[10] A. Eirin, X.Y. Zhu, S. Jonnada, A. Lerman, A.J. van Wijnen, L.O. Lerman, Mesenchymal stem cell-derived extracellular vesicles improve the renal microvasculature in metabolic renovascular disease in swine, Cell Transplant. 27 (7) (2018) 1080–1095, https://doi.org/10.1177/0963689718780942.
[11] X.Y. Liao, M. Chen, Y. Zhang, S.C. Li, Y.J. Li, Y. He, Y.T. Zhao, L.H. Luo, Platelet lysate promotes proliferation and angiogenic activity of dental pulp stem cells via store-operated Ca2+ entry, Nano TransMed (2023) 100021, https://doi.org/10.1016/j.ntm.2023.100021. ISSN 2790-6760.
[12] A.A. Albashari, Y. He, Y. Luo, X. Duan, J. Ali, M. Li, D. Fu, Y. Xiang, Y. Peng, S. Li, et al., Local spinal cord injury treatment using a dental pulp stem cell encapsulated H2S releasing multifunctional injectable hydrogel, Adv. Healthcare Mater. 13 (9) (2024) e2302286, https://doi.org/10.1002/adhm.202302286.
[13] Y. He, R. Li, W. She, Y. Ai, K. Li, T. Kumeria, Z. Jiang, Q. Shao, C. Zou, A.A. Albashari, et al., Inhibitory effects of the nanoscale lysate derived from xenogenic dental pulp stem cells in lung cancer models, J. Nanobiotechnol. 21 (1) (2023) 488, https://doi.org/10.1186/s12951-023-02218-1.
[14] X.X. Duan, Y. Luo, R. Zhang, H. Zhou, W. Xiong, R.H. Li, Z.Y. Huang, L.H. Luo, S. Rong, M.C. Li, et al., ZIF-8 as a protein delivery system enhances the application of dental pulp stem cell lysate in anti-photoaging therapy, Mater. Today Advan. (2023) 100336, https://doi.org/10.1016/j.mtadv.2022.100336. ISSN 2590-0498.
[15] D.G. Robinson, Y. Ding, L. Jiang, Unconventional protein secretion in plants: a critical assessment, Protoplasma 253 (1) (2016) 31–43, https://doi.org/10.1007/s00709-015-0887-1.
[16] H. Peinado, M. Alečković, S. Lavotshkin, I. Matei, B. Costa-Silva, G. Moreno-Bueno, M. Hergueta-Redondo, C. Williams, G. García-Santos, C. Ghajar, et al., Melanoma exosomes educate bone marrow progenitor cells toward a pro-metastatic phenotype through MET, Nat. Med. 18 (6) (2012) 883–891, https://doi.org/10.1038/nm.2753.
[17] L. Cheng, A.F. Hill, Therapeutically harnessing extracellular vesicles, Nat. Rev. Drug Discov. 21 (5) (2022) 379–399, https://doi.org/10.1038/s41573-022-00410-w.
[18] K.W. Witwer, B.W.M. Van Balkom, S. Bruno, A. Choo, M. Dominici, M. Gimona, A.F. Hill, D. De Kleijn, M. Koh, R.C. Lai, et al., Defining mesenchymal stromal cell (MSC)-derived small extracellular vesicles for therapeutic applications, J. Extracell. Vesicles 8 (1) (2019) 1609206, https://doi.org/10.1080/20013078.2019.1609206.
[19] M. ter Huurne, R. Schelbergen, R. Blattes, A. Blom, W. de Munter, L.C. Grevers, J. Jeanson, D. Noël, L. Casteilla, C. Jorgensen, et al., Antiinflammatory and chondroprotective effects of intraarticular injection of adipose-derived stem cells in experimental osteoarthritis, Arthritis Rheum. 64 (11) (2012) 3604–3613, https://doi.org/10.1002/art.34626.
[20] A. Monsel, Y.G. Zhu, S. Gennai, Q. Hao, S. Hu, J.J. Rouby, M. Rosenzwajg, M.A. Matthay, J.W. Lee, Therapeutic effects of human mesenchymal stem cell-derived microvesicles in severe pneumonia in mice, Am. J. Respir. Crit. Care Med. 192 (3) (2015) 324–336, https://doi.org/10.1164/rccm.201410-1765OC.
[21] J.R. Klinger, M. Pereira, M. Del Tatto, A.S. Brodsky, K.Q. Wu, M.S. Dooner, T. Borgovan, S. Wen, L.R. Goldberg, J.M. Aliotta, et al., Mesenchymal stem cell extracellular vesicles reverse sugen/hypoxia pulmonary hypertension in rats, Am. J. Respir. Cell Mol. Biol. 62 (5) (2020) 577–587, https://doi.org/10.1165/rcmb.2019-0154OC.
[22] B. Yu, M. Gong, Y. Wang, R.W. Millard, Z. Pasha, Y. Yang, M. Ashraf, M. Xu, Cardiomyocyte protection by GATA-4 gene engineered mesenchymal stem cells is partially mediated by translocation of miR-221 in microvesicles, PLoS One 8 (8) (2013) e73304, https://doi.org/10.1371/journal.pone.0073304.
[23] C. Diener, A. Keller, E. Meese, The miRNA-target interactions: an underestimated intricacy, Nucleic Acids Res. 52 (4) (2024) 1544–1557, https://doi.org/10.1093/nar/gkad1142.
[24] C. Gong, Z. Gu, X. Zhang, Q. Xu, G. Mao, Z. Pei, W. Meng, J. Cen, J. Liu, X. He, et al., HMSCs exosome-derived miR-199a-5p attenuates sulfur mustard-associated oxidative stress via the CAV1/NRF2 signalling pathway, J. Cell Mol. Med. 27 (15) (2023) 2165–2182, https://doi.org/10.1111/jcmm.17803.
[25] A. Douvris, J. Viñas, K.D. Burns, miRNA-486-5p: signaling targets and role in non-malignant disease, Cell. Mol. Life Sci.: CM 79 (7) (2022) 376, https://doi.org/10.1007/s00018-022-04406-y.
[26] B. Zhu, W. Liu, Q. Xu, H.L. Liu, MicroRNA-486-5p functions as a diagnostic marker for carotid artery stenosis and prevents endothelial dysfunction through inhibiting inflammation and oxidative stress, Bioengineered 13 (4) (2022) 8667–8675, https://doi.org/10.1080/21655979.2022.2054500.

[27] X.F. Shi, H. Wang, F.J. Xiao, Y. Yin, Q.Q. Xu, R.L. Ge, L.S. Wang, MiRNA-486 regulates angiogenic activity and survival of mesenchymal stem cells under hypoxia through modulating Akt signal, Biochem. Biophys. Res. Commun. 470 (3) (2016) 670–677, https://doi.org/10.1016/j.bbrc.2016.01.084.
[28] A.M. Luks, E.R. Swenson, P. Bärtsch, Acute high-altitude sickness. European respiratory review: an official, J. Europ. Respirat. Soc. 26 (143) (2017) 160096, https://doi.org/10.1183/16000617.0096-2016.
[29] P. Woods, J. Alcock, High-altitude pulmonary edema, Evol. Med. Public Health 9 (1) (2021) 118–119, https://doi.org/10.1093/emph/eoaa052.
[30] J. Vandewalle, A. Luypaert, K. De Bosscher, C. Libert, Therapeutic mechanisms of glucocorticoids, Trends Endocrinol. Metabol.: TEM (Trends Endocrinol. Metab.) 29 (1) (2018) 42–54, https://doi.org/10.1016/j.tem.2017.10.010.
[31] C.K. Lin, Y.H. Lin, T.C. Huang, C.S. Shi, C.T. Yang, Y.L. Yang, VEGF mediates fat embolism-induced acute lung injury via VEGF receptor 2 and the MAPK cascade, Sci. Rep. 9 (1) (2019) 11713, https://doi.org/10.1038/s41598-019-47276-4.
[32] D.Y. Zheng, M. Zhou, J. Jin, M. He, Y. Wang, J. Du, X.Y. Xiao, P.Y. Li, A.Z. Ye, J. Liu, et al., Inhibition of P38 MAPK downregulates the expression of IL-1β to protect lung from acute injury in intestinal ischemia reperfusion rats, Mediat. Inflamm. 2016 (2016) 9348037, https://doi.org/10.1155/2016/9348037.
[33] S.H. Mei, J.J. Haitsma, C.C. Dos Santos, Y. Deng, P.F. Lai, A.S. Slutsky, W.C. Liles, D.J. Stewart, Mesenchymal stem cells reduce inflammation while enhancing bacterial clearance and improving survival in sepsis, Am. J. Respir. Crit. Care Med. 182 (8) (2010) 1047–1057, https://doi.org/10.1164/rccm.201001-0010OC.
[34] D.R. Potter, B.Y. Miyazawa, S.L. Gibb, X. Deng, P.P. Togaratti, R.H. Croze, A.K. Srivastava, A. Trivedi, M. Matthay, J.B. Holcomb, et al., Mesenchymal stem cell-derived extracellular vesicles attenuate pulmonary vascular permeability and lung injury induced by hemorrhagic shock and trauma, J. Trauma Acute Care Surg. 84 (2) (2018) 245–256, https://doi.org/10.1097/TA.0000000000001744.
[35] C. Gao, Y.J. Xu, Z.X. Meng, S. Gu, L. Zhang, L. Zheng, BMSC-derived exosomes carrying lncRNA-ZFAS1 alleviate pulmonary ischemia/reperfusion injury by UPF1-mediated mRNA decay of FOXD1, Mol. Neurobiol. 60 (5) (2023) 2379–2396, https://doi.org/10.1007/s12035-022-03129-2.
[36] J.A. Jefferson, J. Simoni, E. Escudero, M.E. Hurtado, E.R. Swenson, D.E. Wesson, G.F. Schreiner, R.B. Schoene, R.J. Johnson, A. Hurtado, Increased oxidative stress following acute and chronic high altitude exposure, High Alt. Med. Biol. 5 (1) (2004) 61–69, https://doi.org/10.1089/152702904322963690.
[37] S. Paul, A. Gangwar, K. Bhargava, Y. Ahmad, D4F prophylaxis enables redox and energy homeostasis while preventing inflammation during hypoxia exposure, Biomed. Pharmacother. 133 (2021) 111083, https://doi.org/10.1016/j.biopha.2020.111083.
[38] C. Lisk, J. McCord, S. Bose, T. Sullivan, Z. Loomis, E. Nozik-Grayck, T. Schroeder, K. Hamilton, D.C. Irwin, Nrf2 activation: a potential strategy for the prevention of acute mountain sickness, Free Radic. Biol. Med. 63 (2013) 264–273, https://doi.org/10.1016/j.freeradbiomed.2013.05.024.
[39] K.J. Dunham-Snary, D. Wu, E.A. Sykes, A. Thakrar, L.R.G. Parlow, J.D. Mewburn, J.L. Parlow, S.L. Archer, Hypoxic pulmonary vasoconstriction: from molecular mechanisms to medicine, Chest 151 (1) (2017) 181–192, https://doi.org/10.1016/j.chest.2016.09.001.
[40] H. Duplain, L. Vollenweider, A. Delabays, P. Nicod, P. Bärtsch, U. Scherrer, Augmented sympathetic activation during short-term hypoxia and high-altitude exposure in subjects susceptible to high-altitude pulmonary edema, Circulation 99 (13) (1999) 1713–1718, https://doi.org/10.1161/01.cir.99.13.1713.
[41] U. Scherrer, L. Vollenweider, A. Delabays, M. Savcic, U. Eichenberger, G.R. Kleger, A. Fikrle, P.E. Ballmer, P. Nicod, P. Bärtsch, Inhaled nitric oxide for high-altitude pulmonary edema, N. Engl. J. Med. 334 (10) (1996) 624–629, https://doi.org/10.1056/NEJM199603073341003.
[42] T.E. Ingram, A.G. Pinder, D.M. Bailey, A.G. Fraser, P.E. James, Low-dose sodium nitrite vasodilates hypoxic human pulmonary vasculature by a means that is not dependent on a simultaneous elevation in plasma nitrite, Am. J. Physiol. Heart Circ. Physiol. 298 (2) (2010) H331–H339, https://doi.org/10.1152/ajpheart.00583.2009.
[43] S. Taghavi, D. Abraham, P. Riml, P. Paulus, R. Schäfer, W. Klepetko, S. Aharinejad, Co-expression of endothelin-1 and vascular endothelial growth factor mediates increased vascular permeability in lung grafts before reperfusion, J. Heart Lung Transplant. 21 (5) (2002) 600–603, https://doi.org/10.1016/s1053-2498(01)00346-1.
[44] Y. Ke, O.V. Oskolkova, N. Sarich, Y. Tian, A. Sitikov, M.E. Tulapurkar, S. Son, A.A. Birukova, K.G. Birukov, Effects of prostaglandin lipid mediators on agonist-induced lung endothelial permeability and inflammation, Am. J. Physiol. Lung Cell Mol. Physiol. 313 (4) (2017) L710–L721, https://doi.org/10.1152/ajplung.00519.2016.
[45] K. Kobayashi, D. Horikami, K. Omori, T. Nakamura, A. Yamazaki, S. Maeda, T. Murata, Thromboxane A2 exacerbates acute lung injury via promoting edema formation, Sci. Rep. 6 (2016) 32109, https://doi.org/10.1038/srep32109.
[46] Y.P. Hwang, H.G. Jeong, The coffee diterpene kahweol induces heme oxygenase-1 via the PI3K and p38/Nrf2 pathway to protect human dopaminergic neurons from 6-hydroxydopamine-derived oxidative stress, FEBS Lett. 582 (17) (2008) 2655–2662, https://doi.org/10.1016/j.febslet.2008.06.045.
[47] T. Qian, B. Qi, Y. Fei, J. Li, L. Luo, B. Lv, Y. Song, S. Sheng, W. Xiao, X. Huang, et al., PLD2 deletion alleviates disruption of tight junctions in sepsis-induced ALI by regulating PA/STAT3 phosphorylation pathway, Int. Immunopharm. 114 (2023) 109561, https://doi.org/10.1016/j.intimp.2022.109561.